觸媒與緩衝層輔助成長單壁碳奈米管
之結構、特性及成長機制

研究生：王威翔　　　　　　　　　　　　指導教授：郭正次 教授

國立交通大學材料科學與工程研究所

摘要

合成單壁碳奈米管(SWNTs)並有效的控制其結構一直是碳管研究上的瓶頸，而製程溫度更決定了 SWNTs 整合在矽基材元件上的可行性。本研究利用微波電漿化學汽相沉積系統(MPCVD) 和電子迴旋共振化學氣相沉積法(ECR-CVD)，在甲烷與氫氣的氣氛中，搭配使用不同的觸媒與緩衝層材料來開發出能在矽基板上成長單壁碳奈米管(SWNTs)的製程，並探討合成的單壁碳奈米管之結構、特性及成長機制。緩衝層材料包含了厚度為 5~15 nm 的 ZnS-SiO_2、Si_3N_4、TiN 、Al_2O_3、AlN 及 AlON，觸媒材料包含了厚度為 1~10 nm 的 Co、Fe 及新穎的 $CoCrPtO_x$ 觸媒前驅物。這個製程先以物理氣相沉積法(PVD)將緩衝層及觸媒材料沉積在附有 2~3 nm SiO_2 的矽基材上；然後再進行氫氣前處理以及後續的碳管沉積。實驗樣品在每個製程步驟中的結構與特性，使用原子力顯微鏡(AFM) 、X-ray 繞射(XRD)、掃描式電子顯微鏡(SEM)、高解析穿透式電子顯微鏡(HRTEM)、X-ray 光電子頻譜(XPS) 、歐傑電子頻譜(AES) 、拉曼光譜儀(Raman spectroscopy) 和場效發射 I-V 量測儀等儀器來分析。實驗結果得到下列結論:

沉積的碳奈米結構與性質主要由下列製程參數所影響：(i) 緩衝層材料、觸媒材料及他們的厚度，(ii) 緩衝層的表面粗糙度及其與觸媒材料間的交互作用。對Co觸媒而言，在不同的緩衝層材料中，促進根莖成長型的網絡狀SWNTs的優先順序為AlON，Al_2O_3，AlN，其中AlN幾乎沒有效應。然而，對Fe觸媒而言，更多數量的底部成長型之蜷曲狀的SWNTs在使用AlN 與Al_2O_3兩種緩衝層材料下都能生長；而Co和Fe兩種觸媒材料使用非鋁基或是SiO_2的緩衝層都無法生長出碳奈米結構，或是僅能生長多壁碳奈米管(MWNTs)。

對於$CoCrPtO_x$觸媒前趨物而言，使用MPCVD的沈積方法可以在附有SiO_2緩衝層的矽基材上，於600 °C的低溫下成功的長出準直且濃密的底部成長型SWNTs薄膜；有趣的是在AlON緩衝層的輔助下，可以進一步增加碳管的密度及長度(~60 μm)。此外，鍍有觸媒與緩衝層的基材在把合成的碳管取下後仍可重複的使用來成長SWNTs。相較於MPCVD，使用ECR-CVD系統成長出的底部成長型之CNTs則混合著單壁、雙壁與四層管壁(管徑分別為~2.0 nm，3.6 nm 和7.9 nm)，而這樣的管徑也是目前文獻中利用ECRCVD所能合成出的最小管徑。換言之，相較於Fe或Co的觸媒薄膜，$CoCrPtO_x$觸媒前趨物是最有效率的媒介來形成有利於SWNTs成長的小粒徑觸媒粒子，並且在沒有緩衝層的輔助下也能成長出SWNTs。

關於緩衝層與觸媒材料厚度的影響，結果指出緩衝層的厚度(5~15 nm)對於成長之碳奈米結構沒有顯著影響；相較於緩衝層厚度，越薄的觸媒厚度則更容易成長出小尺寸的碳奈米結構。

關於製程溫度與CH_4/H_2流量的影響，結果顯示使用不同觸媒材料來成長SWNTs的最低製程溫度並無明顯不同(Co, ~620 ℃; Fe, ~610 ℃; $CoCrPtO_x$ ~600 ℃)；結果也揭露了最適合的CH_4/H_2流量在Co、Fe與$CoCrPtO_x$觸媒前趨物各為5/50、1.5/200與4/50 (sccm/sccm)，換句話說，相較於底部成長型的CNTs，根莖成長型的CNTs需要最高的碳源濃度。

關於觸媒與緩衝層輔助成長SWNT的生長機制，鋁基緩衝層主要提供下列功能：(1) 在表面上提供適當大小的奈米級孔洞以防止奈米粒子的聚集；(2) 能在較厚的觸媒薄膜上形成奈米突起點以利生長出根莖成長型的SWNTs；(3) 影響觸媒跟緩衝層之間的交互作用力，包含化學鍵結、潤濕性及表面張力；(4) 控制碳源擴散的路徑。在底部成長型的Fe和$CoCrPtO_x$觸媒輔助成長的SWNTs中，鋁基緩衝材料提供了防止顆粒聚集的作用。相對的，鋁基緩衝材料形成奈米突起點的模板作用、與Co觸媒間的高表面張力則促進了根莖成長型的SWNT的生長。此外，鋁基緩衝層也扮演著抑制碳原子擴散到矽基材內部的角色，進而加速碳原子在成長CNTs過程中的其他擴散路徑，這也可能是我們可以在較低的製程溫度下(~600 ℃)合成出SWNT的原因。

關於使用$CoCrPtO_x$觸媒前趨物輔助成長SWNTs的機制，研究中發現$CoCrPtO_x$觸媒前趨物能在氫氣前處理後形成非常細小且分佈均勻的觸媒顆粒(1~3 nm)，這是由於在氫氣前處理時，PtO_x在$CoCrPtO_x$的分解反應會產生爆炸效應而讓觸媒材料形成奈米顆粒，而Cr_2O_3則扮演著阻止奈米觸媒顆粒聚集的角色。AlON緩衝層的主要作用則是利用表面上的孔洞進一步的防止觸媒粒子的聚集，這些綜合的效應使得細小且分佈均勻的奈米觸媒

粒子能夠形成，並隨後長出濃密且準直的SWNTs薄膜。

關於緩衝層輔助成長的奈米碳管的結構與性質，Co觸媒與AlON緩衝層輔助成長之網絡狀SWNTs、Fe觸媒與Al_2O_3和Fe觸媒與AlN輔助成長之蜷曲狀SWNTs的I_G/I_D比分別為~15.7、~10.8與~31.5；這些結果與文獻中所揭露的氮原子在緩衝層或觸媒層中能提高觸媒活性進而得到較高I_G/I_D比的結果一致。而利用$CoCrPtO_x$觸媒前趨物合成之SWNTs薄膜的I_G/I_D比則高達43，其熱重分析結果顯示其在空氣中的抗氧化溫度高達586°C ~ 691°C，此特性與雷射法成長並經純化過的單壁奈米碳管相似；結果也指出使用$CoCrPtO_x$觸媒前趨物在ECRCVD成長出碳管的I_G/I_D比(~0.58)遠不如MPCVD合成的CNTs。關於場發射性質，網絡狀的Co輔助成長CNTs、$CoCrPtO_x$輔助成長SWNTs及Fe觸媒輔助成長之CNTs的起始電壓與最大電流密度分別為＞10、4.6 和 3.4~3.6 V/μm (在電流密度0.01 mA/cm^{2}時)，＜0.01 (在10 V/μm時)、~33 (在6.7 V/μm時) 和 ~34 mA/cm^2 (在5.6 V/μm時)；濃密的$CoCrPtO_x$輔助成長之SWNTs比準直的Fe觸媒輔助成長之CNTs擁有較大的起始電壓是因為屏蔽效應(screening effect)所導致。

總結整個結果，利用Co和Fe作為觸媒可以在適當的緩衝層材料的輔助下成長出一些SWNTs，然而，藉由新穎的$CoCrPtO_x$材料前趨物搭配AlON的緩衝層卻能合成出超過99%純度的SWNTs；這個研究的結果提供了新的思考方式來設計新的製程，以達到操控奈米結構的目的。

Structures, properties and growth mechanisms of the SWNTs synthesized by catalyst and buffer layer-assisted MPCVD

Student : Wei-Hsiang Wang **Advisor : Cheng-Tzu Kuo**

Institute of Materials Science and Engineering
National Chiao Tung University

Abstract

Synthesis and effective control of the nanostructures of single-walled carbon nanotubes (SWNTs) are the current bottlenecks in CNTs researches in which process temperature further determines the feasibility of SWNTs integrated with Si-based devices. In this work, the processes to fabricate catalyst and buffer layer-assisted SWNTs on Si wafer were developed by both microwave plasma–enhanced chemical vapor deposition (MPCVD) and electron cyclotron resonance chemical vapor deposition (ECR-CVD) with different buffer and catalyst materials, using CH_4 and H_2 as source gases. The buffer and catalyst materials include ZnS-SiO_2, Si_3N_4, TiN, Al_2O_3, AlN, and AlON of 5 ~ 15 nm in thickness, and Co, Fe, and novel $CoCrPtO_x$ precursor films of 1 ~10 nm in thickness, respectively. The processes include deposition of the buffer and catalyst material on the native SiO_2 of 2 ~ 3 nm of Si wafer by physical vapor deposition (PVD). The coated substrates were then followed by H-plasma pretreatment before CNTs deposition. The structures and properties after each processing step were characterized by atomic force microscopy (AFM), X-ray diffractometry (XRD), field emission scanning electron microcopy (FESEM), high resolution transmission electron microscopy (HRTEM), X-ray photoelectron spectroscopy (XPS), Auger electron spectroscopy (AES), Raman spectroscopy and field emission I-V measurements. From the experimental results, the following conclusions can be drawn.

The results indicate that the main processing parameters to affect the deposited nanostructures and their properties are: (i) buffer and catalyst materials and their thicknesses, (ii) surface roughness range of buffer layer and its interaction with catalyst materials. For Co as catalyst, the favor tendency to form more root-growth SWNTs networks of different buffer materials are in order of AlON, Al_2O_3 and AlN, in which AlN has no detectable effect. In contrast, for Fe as catalyst, the more amounts of base-growth spaghetti-like SWNTs can be formed with either AlN or Al_2O_3 as buffer layer. The results also found that the multi-walled carbon nanotubes (MWNTs) or amorphous carbon films are merely formed by using non-Al-based materials or the native SiO_2 as buffer material, no matter what Fe or Co acts as

catalyst.

In the case of using $CoCrPtO_x$ catalyst precursor, the vertically aligned base-growth SWNTs films can be successfully fabricated on silicon wafer with native SiO_2 as buffer layer by MPCVD at low temperatures down to ~ 600 ^oC. It is interesting to note that AlON buffer can further increase the tube number densities and their lengths (~ 60 μm). Furthermore, the catalyst- and buffer-coated substrates can be repeatedly used for SWNTs deposition by wiping out the previously deposited CNTs. In contrast to MPCVD, the deposited CNTs by ECR-CVD are the mixing types of base-growth CNTs consisting of SWNTs, double-walled and four-walled-CNTs (~ 2.0, 3.6 and 7.9 nm in diameter, respectively), which are the smallest reported sizes of CNTs in the literature by ECRCVD. On the other hands, the $CoCrPtO_x$ catalyst precursor can be the more effective agent to produce the smaller sized catalysts than directly coated Fe or Co catalysts to grow SWNTs without additional buffer application.

Regarding effects of thickness of buffer and catalyst layers, the results indicate that buffer layer thickness (5 ~ 15 nm) has no significant effects on the deposited nanostructures. In contrast to buffer thickness, it shows that smaller catalyst thickness gives rise to smaller tube diameter of the nanostructures.

Regarding effects of temperature and CH_4/H_2 ratio conditions, the results demonstrate that the lowest temperatures to obtain the SWNTs are about the same (Co, ~620 ℃; Fe, ~610 ℃; $CoCrPtO_x$ ~600 ℃), indicating no significant differences among different catalyst materials. The results appeal that the favorable CH_4/H_2 ratios to grow the smaller sized CNTs or SWNTs for Co, Fe and $CoCrPtO_x$ film are around 5/50, 1.5/200 and 4/50 (sccm/sccm), respectively. In other words, by comparing with the base-growth CNTs, the Co-assisted root-growth SWNTs requires the greatest carbon source concentration.

On growth mechanisms of the buffer- and catalyst-assisted SWNTs, the Al-based buffer layers essentially have the following functions: (1) providing the proper nano-sized dimples on their surface to accommodate the nanoparticles from agglomeration between neighbor nanoparticles, (2) acting as template for the thicker catalyst film to promote formation of nano-sized extrusions for the root growth SWNTs, (3) affecting interactions between catalyst and buffer materials, including chemical bonding formation, wetterability and surface tension of catalyst with buffer material, and (4) varying the diffusion path of carbon during CNTs growth. For accommodating effects, the Al-based buffers can promote the smaller-sized base-growth Fe-assisted and $CoCrPtO_x$-assisted SWNTs. For effects of acting as template and giving a higher surface tension of Co/buffer interface, the Al-based buffers can enhance the root-growth Co-assisted SWNTs, instead of base-growth Fe-assisted SWNTs. For effect of changing diffusion path, the Al-based buffers can act as the carbon diffusion inhibitor to reduce the possible diffusion path of carbon through Si wafer and to accelerate other carbon diffusion paths during CNTs growth, which may reduce the deposition temperature (~600 ℃) of SWNTs by combining with smaller particle sizes.

For the case of $CoCrPtO_x$-assisted SWNTs, formation of very fine catalyst nanoparticles (1~3 nm) after H-plasma pretreatment is demonstrated. This is due to the explosive

decomposition effect of PtO_x in $CoCrPtO_x$ precursor during H-plasma pretreatment. The Cr_2O_3 in precursor may also play a role in inhibiting the agglomeration of alloy catalyst nanoparticles. Effect of AlON buffer in this case is essentially to act as accommodating pores for catalysts to further reduce the agglomeration effect, which causes the denser well-distributed smaller nanoparticles and so SWNTs formations.

With respect to the structures and properties of the as-grown buffer-layer-assisted SWNTs, the Co-assisted SWNT networks with AlON buffer, the spaghetti-like Fe-assisted SWNTs with Al_2O_3 and AlN buffers demonstrate I_G/I_D ratios of ~15.7, ~10.8 and ~31.5, respectively. The results are in agreement with the reported results in the literature that a higher N concentration in the buffer or catalyst may give rise to a higher I_G/I_D ratio by prolonging catalyst activity. In contrast, for $CoCrPtO_x$–assisted SWNTs with AlON buffer, the I_G/I_D ratio can go up to ~ 43 and its TGA results show oxidation resistance up to 586°C ~ 691°C, which are comparable with that for the purified SWNTs synthesized by a laser-oven method. The results also show that the I_G/I_D ratio of the $CoCrPtO_x$-assisted CNTs by ECRCVD is ~ 0.58, which is much lower than 43 for CNTs by MPCVD. On field emission properties, the turn-on voltages are > 10, 4.6 and 3.4 ~ 3.6 V/μm (for current density 0.01 mA/cm^2) and the highest current densities are ＜0.01 (at 10 V/μm), ~33 (at 6.7 V/μm) and ~34 mA/cm^2 (at 5.6 V/μm) for the root-growth Co-assisted CNTs, the $CoCrPtO_x$–assisted SWNTs and the base-growth Fe-assisted CNTs, respectively. The turn-on voltage for the denser $CoCrPtO_x$–assisted SWNTs is higher than that of the well-aligned Fe-assisted CNTs is believed to be due to screening effect.

In summary, some percentages the Co- and Fe-assisted SWNTs can be synthesized and assisted by the application of Al-based buffer layers. However, application of the $CoCrPtO_x$ precursor with AlON buffer can assisted > 99% formation of SWNTs. The results have improved our thinking to design the desired process to obtain the required nanostructures.

Acknowledgements

首先要感謝郭正次老師五年來的悉心指導，想起當初前幾次投稿時老師不厭其煩的修改及教導，連續好幾個星期，每天逐字逐句的修改、討論屢屢從華燈初上直至深夜方才休息，當時的情景至今依然歷歷在目；而老師做學問的態度及方法更是讓我折服不已；這樣的訓練也讓我對於事物的本質能看的更為深邃、透徹，對於在職進修的我而言，這一趟校園取經之旅真的是人生中一場難得的饗宴。而潘扶民教授對於本論文所提出的寶貴意見更是讓我受惠良多。同時也要感謝成大機械系李驊登教授、明道大學副校長陳家富教授、中央機械系林景崎教授、成大化工系洪昭南教授、北科大機電學院院長林啟瑞教授等考試委員的親臨指導。此外，感謝錸德科技王式禹副總的推薦，讓我在工作多年後有重拾書本再度充電的機會；另外，也要特別感謝錸德科技羅慶忠總經理與邱銘中協理對於在職進修的支持。

感謝這五年中曾經與我共同合作過的學弟妹們，國銘、亦同、玉容、蔡豪及崇獻，因為有你們的協助，我們才能不斷的前進，一路從多壁碳管的合成進階到單壁碳管的開發，跟你們一起執行三年期國家奈米計畫真的是非常棒的經驗！感謝伊茹、貞君及必楷在實驗與生活上的協助，因為有你們任勞任怨的張羅實驗室大小事，我們才能心無旁騖的專心在實驗上，還有兆君學長、柏林、志忠、安亞、立群、文綬，宜學、傳恕、盈君、凱齡、淑筠，非常榮幸能夠跟各位作為同一個實驗的伙伴。除此之外，也感謝錸德同事鍾利群與蔡蕙芳在薄膜濺鍍上的協助以及中科院黃信二博士在貴重分析儀器上的大力幫忙。

最後，要特別感謝家人對於在職進修的支持與鼓勵，特別是老婆的支持，將兩個兒子及家庭照顧得非常好，讓我能心無旁騖的完成學業。

Contents

Chinese abstract……………………………………………………………………..............I

English abstract……………………………………………………………………….…...VI

Acknowledgements...............…………………….. VII

Contents...................………………………...VIII

List of symbols…………………………….……………………………….……………….. XI

Table captions...........………………………………...XIII

Figure captions…………………………….…………………………………………………...XV

Chapter 1 Introduction…………………………………………………………..........1

1.1 Background ……………………………………….…….…..……….…..…...…1

1.2 Motivation……….……………………………………………………..….……....3

Chapter 2 Literture review…..5

2.1 Structures and properties of SWNTs.………………………………...…...….……5

2.2 Synthetic methods of SWNTs.…………………………………….…..….……..8

2.3 Structures and process parameters of as-grown SWNTs by catalytic-CVD………12

2.4 The proposed Growth mechanisms of SWNTs……………………..……….….…14

2.5 Analytical method of SWNTs……………………….…………………….....21

2.6 Applications of SWNTs………………………………...……….……….....24

Chapter 3 Experimental methods………………………………..…………………...31

3.1 Experimental flow chart……………………………………………..… ……31

3.2 Raw materials……….…………………………………………………...… ……32

3.3 Depositions of catalyst and buffer layer thin films ……………………….………32

3.4 Design principle of $CoCrPtO_x$ as catalyst precursor...…………………………….…33

3.5 Microwave plasma chemical vapor deposition system (MPCVD)………………..…35

3.6 Electron cyclotron resonance chemical vapor deposition system (ECR-CVD)…….36

3.7 Pretreatment and growth procedures of CNTs……………………..……………….37

3.8 Analyses of structures and properties ……………………………...........………43

Chapter 4 Results and discussion ……………………………………..…………....48

4.1 Characteristics of buffer layer………………………………….………………48

4.2 Morphologies of catalyst film after hydrogen pretreatment………..…………......51

4.2.1 Morphologies of the pre-treated Co catalyst films by MPCVD……………......51

4.2.2 Morphologies of the pre-treated Fe catalyst films by MPCVD……………..…54

4.2.3 Morphologies of the pre-treated $CoCrPtO_x$ films by MPCVD……….…...…57

4.2.4 Morphologies of the pre-treated $CoCrPtO_x$ films by ECRCVD……….……...60

4.3 Structures of the Co-assisted carbon nanostructures by MPCVD……………...…65

4.3.1 Effects of buffer layer materials and catalyst thickness……….……….……...65

4.3.2 Effects of pressure…………………………………………………………69

4.3.3 TEM microstructures ………………..……………………..………………..71

4.4 Structures and properties of Fe-assisted carbon nanostructures by MPCVD………74

4.4.1 Effects of buffer layer materials, CH_4/H_2 ratio and catalyst thickness……...74

4.4.2 Effect of Al_2O_3 and AlN thickness……………………………………….…80

4.4.3 TEM microstructures……………………………………………………85

4.4.4 Field emission properties ……..………………….…………………………85

4.4.5 Role of nitrogen ……………..……………..……………………………..86

4.5 Structures and properties of the CoCrPtOx-assisted carbon nanostructures by MPCVD…………………………………………………………………89

4.5.1 Morphologies and Raman spectra ……………………………….………..89

4.5.2 TEM microstructures………………………..………………………...……..93

4.5.3 Field emission properties and TGA..…………………………………………95

4.6 Structures of the as-grown CoCrPtOx-assisted carbon nanostructures by ECR-CVD……………………………………………………………………..97

4.6.1 Morphologies and Raman spectra ……………………………………...……97

4.6.2 TEM microstructures………………………….………………..……….……97

4.7 My proposed growth mechanisms of SWNTs……………………………..101
4.7.1 Growth mechanism of network-like Co-assisted SWNTs ………………….101
4.7.2 Growth mechanism of spaghetti-like Fe-assisted SWNTs……………………105
4.7.3 Growth mechanism of the CoCrPtOx-assisted SWNTs ……………………...107
4.7.4 Effect of specimens stacking sequences……………………………………..113
4.8 Comparison of various catalyst-assisted carbon nanostructures…………………..115
4.8.1 Role of buffer layer …………………………………………………………115
4.8.2 Raman spectra and field emission properties…………………………….116
4.8.3 Process conditions and synthetic methods…………………………………117
Chapter 5 Conclusions..…………………...……….....................…….........…............120
Chapter 6 Future Prospects………………...………………………..……………………123
References………………………………………………………………………………124
Vita……………………………………………………………………………………136

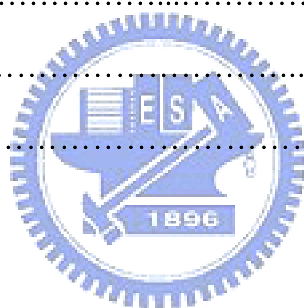

List of symbols

Symbol	Description
AES	Auger electron spectra
AFM	Atomic force microscopy
BSE	Backscattered electron
α	Effective emission area
β	Field enhancement factor
c	Speed of light
C_h	Chiral vector
CNTs	Carbon nanotubes
CRT	Cathode-ray tube
CVD	Chemical vapor deposition
DWNT	Double-walled carbon nanotubes
E	Electron field
ECRCVD	Electron cyclotron resonance chemical vapor deposition
ED	Electron diffraction
EDX	Energy-Dispersive X-Ray
FED	Field emission display
FE-SEM	Field emission scanning electron microscopy
FET	Field effect transistor
FIB	Focused ion beam
FN	Fowler-Nordheim
h	Planck constant
θ	Chiral angle
HRTEM	High resolution transmission electron microscopy
I	Field emission current
J	Field emission current density
LCD	Liquid crystal display
MWNTs	Multi-walled carbon nanotubes
MPCVD	Microwave plasma chemical vapor deposition
NIP	Nano-indentation probe
PDP	Plasma display panel
PVD	Physical vapor deposition
RBM	Radial breathe mode

RF	Radio frequency
SE	Secondary electron
SEM	Scanning electron microscopy
STM	Scanning tunneling microscope
SWNTs	Single-walled carbon nanotubes
TEM	Transmission electron microscopy
TGA	Thermal gravimetric analysis
V	Voltage
XPS	X-ray photoelectron spectroscopy
ϕ	Work function

Table Caption

Table 2-1 General characteristics and synthetic method of as-deposited SWNTs using various catalyst and buffer layer materials in previous study…………………13

Table 3-1 Deposition conditions of catalyst and buffer layer thin films………………..33

Table 3-2 Specimen designations and their process conditions of the Co-assisted nanostructures on Si wafer with various buffer layer materials by MPCVD……………………………………………………………………40

Table 3-3 Specimen designations and their process conditions of the Fe-assisted nanostructures on Si wafer with various buffer layer materials by MPCVD…………………………………………………………………..…41

Table 3-4 Specimen designations and their process conditions of nanostructures on Si wafer using $CoCrPtO_x$ catalyst precursor, where Co and $CoCrO_x$ are used for comparison………………………………………………………………………42

Table 4-1 Roughness of buffer layer films on Si wafer (AFM) ………………………48

Table 4-2 Catalyst particle sizes after H-plasma pretreatment with various buffer layer, and catalyst materials and application methods…………………...……………63

Table 4-3 Summaries of the Co-assisted carbon nanostructures on Si wafer with various buffer layer materials……………………………………………………………..73

Table 4-4 Summaries of the Fe-assisted carbon nanostructures on Si wafer with various buffer layer materials. …………………...……………………………………80

Table 4-5 Summaries of the Fe-assisted carbon nanostructures on Si wafer with various thicknesses of Al_2O_3 and AlN buffer layers.…………………...………………84

Table 4-6 Summaries of the $CoCrPtO_x$–assisted carbon nanostructures on Si wafer with various catalyst thickness and buffer layer. ……………………………………92

Table 4-7 Summaries of the $CoCrPtO_x$–assisted carbon nanostructures on Si wafer by ECRCVD. ………………………………………………………………..100

Table 4-8 Compositions of CoCrPt target, as-deposited $CoCrPtO_x$ film and pretreated $CoCrPtO_x$ film on Si wafer by XPS depth analysis..108

Table 4-9 Summaries of as-deposited carbon nanostructures on Si wafer with various catalyst and buffer layer materials. 119

Figure Caption

Figure 2-1 (a) Graphite sheet, and (b) formed CNT rolled by the graphite sheet[Dresselhaus-1996-p756] [Saito-92-2204] 5

Figure 2-2 The construction of CNT from a single graphite sheet [Saito-1992-2204]..........7

Figure 2-3 The relation between properties and structure of CNTs[Saito-1992-2204]..........7

Figure 2-4 Schematic diagram of arc-discharge system[Saito-1995-33]..........9

Figure 2-5 Schematic diagram of laser ablation system[Guo-1995-49]..........10

Figure 2-6 Schematic drawings of thermal CVD system[Lee-2001-245]..........11

Figure 2-7 Schematic diagram of ball-and-stick scooting model [Birkett-1997-111]..........15

Figure 2-8 TEM image of radiate sea-urchin-like SWNTs[saito-1994-L526]..........16

Figure 2-9 Schematic diagram of root growth mechanism -1[saito-1994-L526]..........16

Figure 2-10 TEM image of the interface between the multilayered cage and the single-walled tube[zhou-1994-1593]..........18

Figure 2-11 Schematic diagram of root growth mechanism -2[Gavillet-2001-275504]..........18

Figure 2-12 Schematic diagram of yarmulke mechanism[Dai-1996-471]..........19

Figure 2-13 Schematic diagram of Solid–liquid–solid growth mechanism[Gorbunov-2002-113]..........20

Figure 2-14 (a) SWNT, (b) double-walled CNT, (c) three-walled CNT, (d) four-walled CNT, and (e) five-walled CNT [成惠民-2004-p. 30]..........21

Figure 2-15 Raman-active normal mode eigenvectors and frequencies for a (10,10) nanotube[Rao-1997-187]..........23

Figure 2-16 Raman spectra of SWNTs[Raravikar-2002-235424]..........23

Figure 2-17 FED display at color mode with red, green, and blue phosphor column[Choi-1999-3129]……………………..………………………..………25

Figure 2-18 Schematic drawing (a) and physical object (b) of a longitudinal cross section of a CRT fluorescent display with a field emission cathode composed of carbon nanotubes [Saito-1998-L346]……………..…..……………25

Figure 2-19 CNTs-based FET Structure and SEM image of a Spindt-type field emitter Two probe I-V_{bias} curve for various values of the gate voltage from a CNTs-based FET[Sander-1998-49]…………………..…………...…………26

Figure 2-20 (a) Atomic Force Microscopy (AFM) image shows the design of the voltage inverter, and (b) Characteristics of the resulting intra-molecular voltage inverter[Derycke-2001-453]………………………..….…………….….27

Figure 2-21 (a) Schematic representation, and (b) image depicting the composition of fabricated SWNT – P3OT flexible solar cells[Landi-2005-165]…………..…....29

Figure 2-22 SWNT attached to the pyramidal tip of a silicon cantilever for AFM[Dai-1996-147]……………………………………………………………30

Figure 2-23 (a)Tapping mode AFM image of a 400-nm-wide, 800-nm-deep trench taken with a bare pyramidal tip, and (b) The image taken with a nanotubes attached to the pyramidal tip with the same specimen[Dai-1996-147]…………30

Figure 3-1 Experimental flowchart…………………………………………………31

Figure 3-2 TEM images of PtO_x thin film after laser pretreatment where small-sized self-assembled Pt nanoparticles are formed…………………………...34

Figure 3-3 Thermo-optical properties of PtO_x single layer…………………….…..35

Figure 3-4 Schematic drawing of MPCVD system…………………………………...36

Figure 3-5 Schematic diagram of ECR-CVD system…………………………….…..37

Figure 3-6 Schematic diagram of specimen stacking sequences..................39

Figure 3-7 Schematic diagram of the field emission measurement setup......46

Figure 4-1 AFM micrographs of the native SiO_2 on Si wafer. : (a) top-view, and (b) scanning profile of roughness..49

Figure 4-2 AFM micrographs of the as-deposited AlN on Si wafer. : (a) top-view, and(b) scanning profile of roughness..49

Figure 4-3 AFM micrographs of the native Al_2O_3 on Si wafer. : (a) top-view, and (b) scanning profile of roughness..50

Figure 4-4 AFM micrographs of the native AlON on Si wafer. : (a) top-view, and (b) scanning profile of roughness..50

Figure 4-5 SEM micrographs of the Co catalyst films (5 nm) after H-plasma pretreatment on silicon wafers with various materials as buffer layers : (a) native SiO_2, (b) ZnS-SiO_2, (c) Al_2O_3, (d) AlN, and (e) AlON, respectively...52

Figure 4-6 SEM micrographs of the Co catalyst films (10 nm) after H-plasma pretreatment on silicon wafers with various materials as buffer layers : (a) native SiO_2, (b) ZnS-SiO_2, (c) Al_2O_3, (d) AlN, and (e) AlON, respectively..53

Figure 4-7 SEM micrographs of the Fe catalyst films (5 nm) after H-plasma pretreatment on silicon wafers with various materials as buffer layers : (a) native SiO_2, (b) Si3N_4, (c) TiN, (d) Al_2O_3, and (e) AlN, respectively......55

Figure 4-8 SEM micrographs of the Fe catalyst films (10 nm) after H-plasma pretreatment on silicon wafers with various materials as buffer layers : (a) native SiO_2, (b) Al_2O_3, and (c) AlN, respectively...........................56

Figure 4-9 SEM micrographs of the $CoCrPtO_x$ precursor films with various thickness after H-plasma pretreatment on silicon wafers with native SiO_2 as buffer layer : (a) 10 nm, (b) 5 nm, (c) 3 nm, (d) 2 nm, (e) 1 nm, and (f) 1 nm, respectively, except (f) with 10 nm AlON as buffer layer……………….58

Figure 4-10 (a) Top-view HRTEM micrograph of $CoCrPtO_x$ precursor nanoparticles following H-plasma treatment, showing uniform and close arrangement. (b) The cross-sectional HRTEM micrograph indicates that the sizes of the nanoparticles range from 2.5 to 3.5 nm……………….……………..….59

Figure 4-11 (a) The cross-sectional HRTEM micrograph of $CoCrPtO_x$ precursor nanoparticles following H-plasma treatment, showing close arrangement and highly distribution density, and (b) the highly magnified image in (a) indicates that the sizes of the nanoparticles range from 1.0 to 3.5 nm…....59

Figure 4-12 SEM micrographs of the $CoCrPtO_x$ precursor with various thickness following H-plasma pretreatment by ECRCVD on silicon wafers with native SiO_2 as buffer layer : (a) 2 nm, (b) 1 nm, and (c) 1 nm, with 10 nm AlON as buffer layer, respectively……………………………………61

Figure 4-13 (a) The top-view HRTEM micrograph of $CoCrPtO_x$ precursor nanoparticles (with native SiO_2 as buffer layer) following H-plasma treatment by ECRCVD, showing a dispersed distribution density, and (b) the highly magnified image in (a) indicates that the sizes of the nanoparticles range from 2.0 to 6.0 nm…………………………………………………....62

Figure 4-14 (a) The top-view HRTEM micrograph of $CoCrPtO_x$ precursor nanoparticles (with AlON as buffer layer) following H-plasma treatment, showing a moderate distribution density, and (b) the highly magnified image in (a) indicates that the sizes of the nanoparticles range from 2.0 to 4.0 nm…....62

Figure 4-15 SEM micrographs of the Co-assisted carbon nanostructures (Co: 5 nm) on silicon wafers with various buffer materials : (a) native SiO_2, (b) ZnS-SiO_2, (c) Al_2O_3, (d) AlN, and (e) AlON, respectively (Specimens A1 to E1)…...66

Figure 4-16 Raman spectra of the Co-assisted carbon nanostructures (Co: 5 nm) on silicon wafers with various buffer materials……………….……..………67

Figure 4-17 SEM micrographs of the Co-assisted carbon nanostructures (Co: 10 nm) on silicon wafers with various buffer materials: (a) native SiO_2, (b) ZnS-SiO_2, (c) Al_2O_3, (d) AlN, and (e) AlON, respectively (Specimens A2 to E2)…...68

Figure 4-18 Raman spectra of the Co-assisted carbon nanostructures (Co: 5 and 10 nm) on silicon wafers with Al_2O_3 and AlON materials as buffer layers.….69

Figure 4-19 SEM micrographs of the Co-assisted carbon nanostructures (Co: 5 nm) with AlON as buffer layer on silicon wafers under different working pressures: (a) 23 Torr, and (b) 16 Torr (Specimens E3 and E4)…………..70

Figure 4-20 Raman spectrum of the Co-assisted carbon nanostructures (Co: 5 nm) with AlON as buffer layer on silicon wafers under 23 Torr of working pressure (Specimens E3)…………………………………………………………70

Figure 4-21 HRTEM images of SWNTs networks grown on silicon wafers with AlON buffer layer : (a) the networks of bundles of SWNTs, and (b) networks are formed by individual SWNT. ………………………………..…..…….72

Figure 4-22 SEM micrographs of the Fe-assisted carbon nanostructures (Fe : 5 nm) on silicon wafers with various buffer materials: (a) native SiO_2, (b) Si_3N_4, (c) TiN, (d) Al_2O_3, and (e) AlN, respectively (Specimens FA1, FB1, FC1, FD1, and FE1)... ……..……..…………………………..………………75

Figure 4-23 Raman spectra of the Fe-assisted carbon nanostructures (Fe: 5 nm) on silicon wafers with native SiO_2, Al_2O_3 and AlN materials as buffer layers

(Specimens FA1, FD1, and FE1). ……………………………..…………76

Figure 4-24 SEM micrographs of the Fe-assisted carbon nanostructures (Fe: 5 nm) on silicon wafers with various buffer materials under a CH_4/H_2 ratio of 5/50 (sccm/sccm): (a) native SiO_2, (b) AlN, (c) Al_2O_3, (d) native SiO_2, (e) AlN, and (f) Al_2O_3, respectively (Specimens FA2, FE2, FD2, FA3, FE3 and FD3)……………………………………………………………..…77

Figure 4-25 Raman spectra of the Fe-assisted carbon nanostructures (Fe: 5 nm) on silicon wafers with native SiO_2, Al_2O_3 and AlN materials as buffer layers under a CH_4/H_2 ratio of 1.5/50 (sccm/sccm) (Specimens FA2, FD2, and FE2) ……………………………………………………………………78

Figure 4-26 Raman spectra of the Fe-assisted carbon nanostructures (Fe: 5 nm) on silicon wafers with native SiO_2, Al_2O_3 and AlN materials as buffer layers under a CH_4/H_2 ratio of 1.5/100 (sccm/sccm) (Specimens FA3, FD3, and FE3)……………………………………………………………………..…78

Figure 4-27 Raman spectra of the Fe-assisted carbon nanostructures (Fe: 10 nm) on silicon wafers with native Al_2O_3 and AlN materials as buffer layers at a CH_4/H_2 ratio of 1.5/100 (sccm/sccm) (Specimens FD6, and FE6). …….79

Figure 4-28 FESEM micrographs of the Fe-assisted carbon nanostructures (Fe: 5 nm) on silicon wafers with various thicknesses of buffer layers: (a) AlN (5 nm), (b) Al_2O_3 (5 nm), (c) AlN (10 nm), (d) Al_2O_3 (10 nm), (e) AlN (15 nm), (f) Al_2O_3 (15 nm), respectively (Specimens FE7, FD7, FE8, FD8, FE9 and FD9). ……………………………………………………………………82

Figure 4-29 Raman spectra of the Fe-assisted carbon nanostructures (Fe: 5 nm) on silicon wafers with different thicknesses of Al_2O_3 buffer layers at a CH_4/H_2 ratio of 1.5/200 (sccm/sccm) (Specimens FD7, FD8, and FD9)... ……….81

Figure 4-30 Raman spectra of the Fe-assisted carbon nanostructures (Fe: 5 nm) on silicon wafers with different thicknesses of AlN buffer layers at a CH_4/H_2 ratio of 1.5/200 (sccm/sccm) (Specimens FE7, FE8, and FE9). …...…….83

Figure 4-31 Typical HRTEM micrograph of the Fe-assisted CNTs (Specimen FE3), in which CNTs consist of SWNTs, DWNTs and MWNTs. ……………….85

Figure 4-32 Field emission I-V curves for the Fe-assisted CNT with native SiO_2, Al_2O_3, and AlN as buffer layers (Fe, 5 nm; CH_4/H_2, 50/5 sccm/sccm). …...…….86

Figure 4-33 **(a)** Auger depth profile as a function of etching time for the pretreated Fe/AlN/Si substrate, and **(b)** Auger electron spectra as a function of etching time for the pretreated Fe/AlN/Si substrate …………………...……….88

Figure 4-34 FESEM micrographs of the $CoCrPtO_x$ –assisted carbon nanostructures on silicon wafers (native SiO_2) with various thicknesses of catalyst layers: (a) 10 nm), (b) 5 nm, (c) 3 nm, (d) 2 nm, (e) 1 nm, and (f) 1 nm (with AlON buffer layer), respectively……………………………………………………90

Figure 4-35 Raman spectra of the $CoCrPtO_x$ –assisted carbon nanostructures on silicon wafers (native SiO_2) with various thicknesses of catalyst layers: (a) 10 nm), (b) 5 nm, (c) 3 nm), (d) 2 nm, (e) 1 nm), and (f) 1 nm (with AlON buffer layer), respectively. ………………………………………91

Figure 4-36 Typical FE-SEM micrographs of extremely dense and vertically aligned $CoCrPtO_x$ –assisted SWNTs films: (a) cross-sectional view, (b) tilt-view and (c) highly magnified image of (b). ……………………………...…91

Figure 4-37 Typical SEM micrograph of $CoCrPtO_x$ –assisted SWNTs films removed from silicon wafer, showing very flexible morphology………………….92

Figure 4-38 HRTEM images : (a) typical bundle-rich SWNTs, (b) SWNT with a diameters of ~ 3 nm, and (c) DWNT with a diameter of ~ 4 nm ..…..….94

Figure 4-39 HRTEM images of typical SWNTs : (a) most of the tubes are of the bundle type, and (b) the highly magnified image of SWNTs shows that their diameters ranges from 2.5 to 3.0 nm. ……………………..……….95

Figure 4-40 Field emission I-V curves for the $CoCrPtO_x$–assisted SWNTs films with AlON as buffer layers (Specimen G6). …………………………..…….96

Figure 4-41 TGA curve of the $CoCrPtO_x$–assisted SWNTs films in air (heating rate is $10^{o}C$/min)……………………………………………………………....96

Figure 4-42 FESEM micrographs of the $CoCrPtO_x$ –assisted carbon nanostructures on silicon wafers (native SiO_2) with various thicknesses of catalyst layers and working pressures: (a) 2 nm, $4x10^{-3}$ Torr (b) 2 nm, $4x10^{-2}$ Torr (c) 2 nm, $4x10^{-1}$ Torr (d) 2 nm, 4 Torr (e) 1 nm, 4 Torr and (f) 1 nm with AlON buffer layer, 4 Torr, respectively. ………………………………………..……….98

Figure 4-43 HRTEM images of typical CNTs : (a) 4-wall MWNT (~7.9 nm), (b) DWNT with a diameters of ~ 3.6 nm, and (c) SWNT with a diameter of ~ 3 nm……………………………………………………………………..99

Figure 4-44 XPS spectrum of as-deposited Co-assisted carbon nanostructures on silicon wafer with AlON as buffer layer……………………………………103

Figure 4-45 Hypothetical growth process of network-like root-growth Co-assisted SWNTs at low temperature by MPCVD. ……………………………….104

Figure 4-46 EDX analysis of the Fe-assisted CNTs film on Si wafer : (a) top of CNTs film, no Fe signal is detected, and (b) bottom of CNTs film, Fe signals are detected indicating Fe catalyst particles remained on Si wafer after CNTs growth. ………………………………………………………………106

Figure 4-47 Hypothetical growth process of spaghetti-like Fe- and buffer-assisted SWNTs by MPCVD…………………………….…………………….107

Figure 4-48 XPS spectra of the $CoCrPtO_x$-coated substrates before and after H-plasma pretreatment for various element or compound in the film : (a) Pt, PtO_x (b) Cr_2O_3, CrO_x and (c) Co, CoO. Upper curves refer to as-deposited films and lower curves represent the pre-treated films……………………….……109

Figure 4-49 Typical FE-SEM micrographs of various H-plasma pretreated catalysts: (a) pure Co, (b) $CoCrO_x$ and (c) $CoCrPtO_x$ thin film………………………111

Figure 4-50 EDX analysis of the substrate-side of the $CoCrPtO_x$-assisted SWNTs film on Si wafer………………………………………………………….112

Figure 4-51 Top-view FE-SEM micrograph of the $CoCrPtO_x$-assisted SWNTs films on the used substrate by wipping out the previously deposited CNTs films……………………………………………………………….113

Figure 4-52 Top-view OM images of effects of specimens stackings: (a) catalyst-coated side of substrate facing plasma, and (b) catalyst-coated side of substrate facing specimen holder……………..……………………………...….114

Figure 4-53 Field emission I-V curves for the Fe-assisted CNTs, the $CoCrPtO_x$ and AlON-assisted SWNTs films, the $CoCrPtO_x$ -assisted CNTs (ECRCVD) and the root-growth Co-assisted CNTs…………………………..……117